EXPERIMENTAL AND NUMERICAL INVESTIGATION OF LIQUID FILM COOLING IN SMALL ROCKET ENGINES

S. Soller[*], R. Behr[*], F. Grauer[*], K. Claramunt[‡], C. Dinescu[‡],

D. Fiorini[#], L. Peveroni[#], A. Simonini[#], S. General[§], Ch. Kirchberger[§], F. Strauss[§], J. Steelant[°]

[*]ArianeGroup GmbH, Taufkirchen
[‡]Numeca International, Brussels
[#]von-Karman-Institute for Fluid Dynamics, Rhode-St.-Genèse
[§]Deutsches Zentrum für Luft- und Raumfahrt, Lampoldshausen
[°]European Space Agency, Noordwijk

Abstract

Within the scope of a GSTP project, a Belgian-German research team performed experiments and simulations to characterise the behaviour of a liquid cooling film and to provide benchmark data for simulation models.

The experiments were performed at DLR's M11.1 air vitiator test facility in Lampoldshausen, Germany. Ethanol was used as film coolant. Apart from being a potential renewable hydrocarbon fuel, ethanol is a suitable substitute fluid for monomethyl-hydrazine, which it is currently being used as propellant and film coolant in small liquid rocket engines. Compared to the situation in a real rocket engine, the experiment was designed to simplify the boundary conditions for the simulations by avoiding chemical reactions of the film with the hot gases as far as possible and to limit the phenomena subject to investigation to heat and mass transfer effects of a liquid cooling film subjected to heating and shear forces.

The experimental setup used a planar film injector in a rectangular hot gas duct. Additionally to measurements of the pressure and temperature of the fluids at inlet and outlet of the test section, thermocouples were installed in the film cooled channel wall to provide information on the axial evolution of the film cooling efficiency. Furthermore, the channel provides optical access for non-intrusive measurement techniques. The von-Karman-Institute used this access to apply laser-based measurements of the temperature of the liquid film. DLR used a dedicated Background-Oriented Schlieren (BOS) technique to provide additional information on the evolution of the film thickness.

Several tests have been performed in spring 2019. The test data have been analysed and are currently being used to benchmark simple engineering models as well as high-fidelity CFD models to predict the behaviour of liquid cooling films in rocket engines.

Abbreviations, Acronyms & Symbols

α	Ramp angle	$\dot{m}$	Mass flow rate [g/s], [kg/s]
BOS	Background-Oriented Schlieren	M	Blowing ratio [-]
CAD	Computer Aided Design	MMH	Monomethylhydrazine
CFD	Computational Fluid Dynamics	p	Pressure [bar]
DLR	Deutsches Zentrum für Luft- und Raumfahrt	ρ	Density [kg/m³]
ESA	European Space Agency	t	Thickness [mm]
H, h	Height [mm]	T	Temperature [K]
L	Length [mm]	v	Velocity [m/s]
LIF	Laser-induced Fluorescence	W	Width [mm]

1   Introduction

1.1   Motivation

Liquid film cooling for rocket engines is an evident possibility to combine the injection of the fuel with an effective method to protect the inner combustor wall surfaces from the hot gas flow. Especially small rocket engines with an unfavourable small ratio of combustor volume to wall surface area use this technology to protect the combustion chamber wall from the hot combustion gases. For very small engines, where the propellant mass flow rates are too small to provide a regenerative cooling of the combustion chamber wall, this is often the only technology to provide a reliable means to limit the wall temperature of the combustion chamber. Large engines often use local film cooling, e.g. close to the injector face plate or upstream of the convergent section of the exhaust nozzle.

As of today, engineers rely largely on empirical correlations to size and design the film cooling system of small liquid rocket engines. However, the applicability of the correlations in literature often is limited to certain operating conditions, film fluids or combustor or injection configurations. To overcome this shortcoming and to develop a more generic film cooling model, a simplified experiment is required which separates the effects of heat and mass transfer of a shear-driven liquid film from the chemical interaction between combustion gases and fuel film coolant.

1.2   State of the Art

Liquid film cooling has been intensively investigated by means of experiments since the mid of the 20th century [1] - [3]. In fact, a significant portion of experimental work relevant for rocket motors was conducted in the 1950s and 1960s [4]. As an example, the comprehensive experimental work of Kinney et al. [5] included the measurement of wall temperature distributions and an optical imaging system applied to a model combustor. Valuable reviews of existing literature on liquid film cooling experiments and simulations are available in references [4], [6] and [7].

In later decades, the majority of published film cooling research focused on the gaseous cooling films within air-breathing propulsion systems, e.g. see the comprehensive synopsis on computational work until 1996 by Kercher [8] or the experimental work of Zuniga et al. [9] or Dellimore et al. [10]. Although especially the experimental setups are also valuable, the encountered test cases are obviously not representative enough for the situation within a liquid rocket engine with liquid (not gaseous) internal wall film cooling. An example for an exception is the kerosene combustor at the institute for flight propulsion at the Technische Universität München initiated by the EU-FP6 programme "Aerodynamic and Thermal Load Interactions with Lightweight Advanced Materials for High Speed Flight" (ATLLAS) project [16].

The experiments can be roughly divided into two categories: on the one hand, experimental tests based on modified rocket combustion chambers exist; on the other hand, test rigs have been designed for the investigation of liquid film cooling, which e.g. apply gas generator to provide hot gas flow. The first type of experiment is usually focused on the technological implications of film cooling, for example the effect on the local wall heat flux or the specific impulse of the engine. The second type is usually dedicated to the understanding of the phenomena governing liquid film cooling.

Two general methods for the wall heat flux measurements were used in the past: first, the calorimetric method is applied, which is based on the temperature and pressure difference of cooling water piped through discrete wall segments; second [17], pairs of thermocouples with a radial recess relative to each other are placed in axial direction in order to directly compute the local temperature difference [18], [19]. Furthermore, measurements of liquid film thicknesses and state of the film (waviness) were attempted by means of high speed photography.

Researchers experimented with various cooling fluids between the 1940s and 1960s, including fluids like Freon-113 or liquid ammonia solutions [20]. Later, either the actual fuel was utilized as film coolant, or liquid water was applied [21]. From a modelling point of view, water provides the advantage that combustion with the hot gas does not need to be taken into account for modelling.

A further parameter encountered in the tests is the location of film injectors and the angle at which the film is injected into the chamber. Moreover, the operating pressures and chamber temperatures vary across a relatively large range. In addition, the Mach number of the investigated flow varies across the tests. Whilst most experiments have been conducted with subsonic core flows, there also exist investigations of film cooling in the nozzle section of rocket combustor, e.g. [22].

The major parameters, in which the experiments available in literature vary, can be listed as follows:

- Reacting vs. non-reacting hot gas flow
- Reacting vs. non-reacting film fluid
- Film cooling injection method
- Liquid film vs. gaseous film
- Thermodynamic state: subcritical, transcritical, supercritical
- Accelerated flow vs. constant-velocity flow
- Temporal length of test runs: few seconds vs. long runs with stabilization of measured quantities
- Vector of film injection
- Reynolds number
- Injected film mass flow rate
- Chamber pressure and temperature

The design of the new film cooling experiment aims at providing additional and more accurate data of liquid film cooling in small rocket engines.

1.3   Experimental Requirements

To close gaps in the already existing and published experimental data base, the test case is intended to serve as a validation reference for CFD w.r.t. predicting the heating and vaporization of a liquid film in a shear driven flow. The test case is supposed to separate the film heating and vaporization process from other processes usually encountered in rocket thrust chambers, like chemical reactions or the impingement of liquid droplets or jets on the combustion chamber wall.

The film fluid and the operating conditions shall be representative of the situation in a small rocket engine using storable liquid fuels like monomethylhydrazine (MMH) or ethanol. Figure 1 compares the thermal and transport properties of MMH with ethanol and water as potential substitute fluids. Ethanol was selected as substitute film fluid due to its similarity in properties when compared to MMH: Surface tension, heat of vaporization and thermal conductivity are quite similar to MMH. Unlike MMH, ethanol does not decompose exothermally at elevated temperatures; this simplifies the experiment, allows to exclude additional chemical effects from the modelling and to focus on the interaction of the shear-driven cooling film with the hot gas. Additionally, ethanol provides the advantage of being a potential rocket fuel itself, especially in the light of the efforts to reduce the use of harmful substances like hydrazine or its derivatives in future hypergolic rocket propellant combinations.

The experimental setup shall allow for representative flow conditions with respect to the velocity of the hot gas flow as well as of the cooling film. Hence, a subsonic gas flow at moderate Mach numbers was envisaged. The use of ethanol as film coolant at subcritical operating conditions resulted in operating conditions which are quite moderate for a typical rocket combustor: hot gas shall be provided at temperatures between 500 K and 600 K. The limitation to 600 K avoids the risk of auto-ignition with the oxidiser in the hot gas flow. To investigate the effect of the pressure on the heat transfer process, two different pressure levels shall be tested, namely ambient pressure and 2 bar.

To provide detailed information on the evolution of the liquid cooling film with respect to its thickness and temperature evolution along the wall, the experimental channel shall provide optical access at several positions. The channel wall shall feature interfaces to install thermocouples to measure the channel's wall temperature.

The interfaces of the setup shall comply with the interface conditions of the M11.1 test facility of DLR in Lampoldshausen, which has been selected for performing the tests.
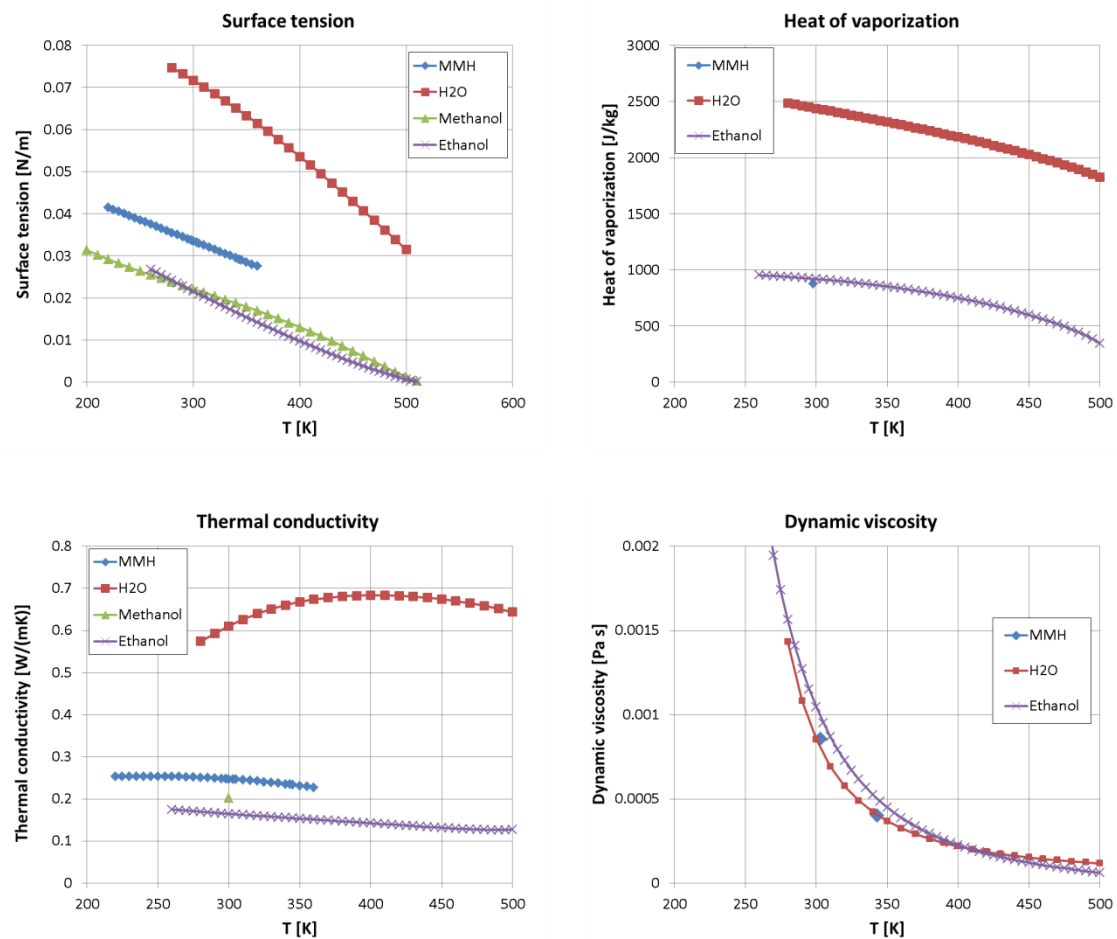
Figure 1: Thermal and transport properties of potential liquid film fluids

2 Experimental Setup

The tests were performed at the M11.1 test facility of DLR in Lampoldshausen. For details on the M11.1 air vitiator and its repeatability of boundary conditions refer e.g. to [23] and [24]. The design of the experimental setup is described in detail in the following sections.

2.1 Channel Design

Figure 2 shows a schematic of the test setup. Compressed air is heated with a hydrogen-fuelled chemical air-vitiator (pre-heater). The hot air is piped to an approach section which transforms the circular cross section of the preheater duct to the rectangular shape of the test section and which ensures the required homogeneity of the inflowing gas at the start of the test section. The test section itself comprises the film injector and the channel housing featuring optical access and the channel floor with thermocouples. In order to allow for an adaptation of the chamber pressure independently of the temperature and pressure of the hot gas flow, a variable exhaust section is installed at the channel's exit.
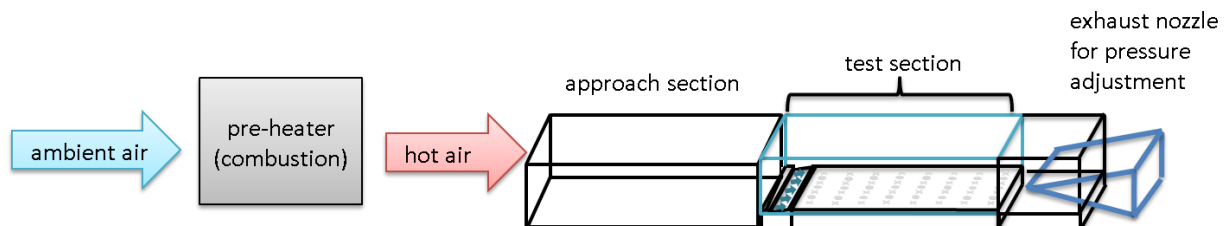

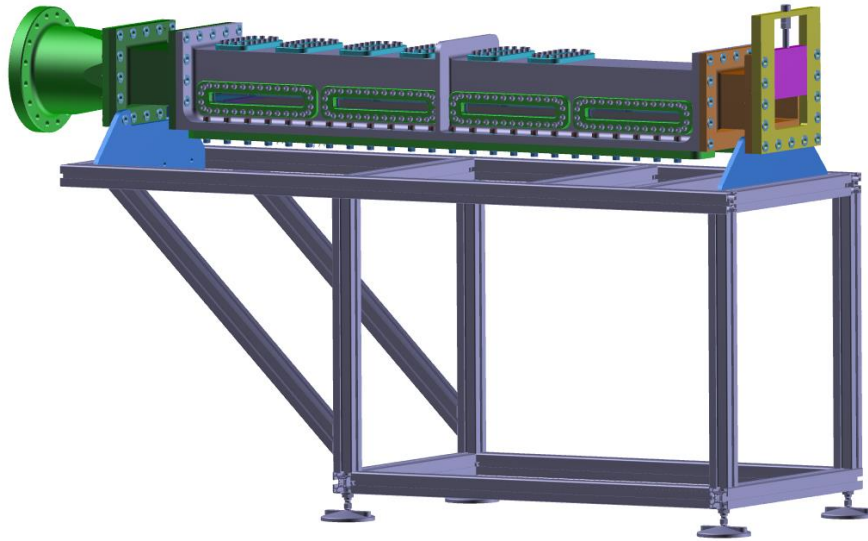Figure 2: Functional schematic of test setup

Figure 3: CAD view of the test setup installed on a support rig

Table 1: Geometry of the test section

Parameter	Symbol	Value	Comment
Channel length	L_{test}	1.0 m	Long enough to ensure film dry-out point is within test section
Channel width	W_{test}	0.12 m	Max. width limited by LIF measurements and max. $\dot{m}_{hotgas}$ of facility
Channel height	H_{test}	0.08 m	Depends on max. $\dot{m}_{hotgas}$ of facility and boundary layer thickness

The actual design of the experimental setup is illustrated in Figure 3. The approach section, which comprises the transition piece to adapt the cross section of the channel and a short settling section to provide a homogeneous inflow profile, is illustrated in green in the CAD view. The subsequent test section is equipped with numerous windows to provide access for optical diagnostics. The exhaust section, comprising a variable-area shutter gate to set the system pressure, is flanged to the right end of the test section. CFD simulations have been performed to assess the flow homogeneity, the evolution of the boundary layer and the effect of the vortex structure upstream of the shutter gate at the exit. The simulations confirmed that the setup provides the required quality of flow conditions for the experiments.

Table 1 lists the geometry of the test section. To allow monitoring the evolution of the film coolant flow in a wide range of mass flow rates, the test section has been designed to stretch across a length of L_{test} = 1 m. The cross section of the channel is given with 12 cm x 8 cm.

Figure 4 shows an overview of the test section. It comprises the channel housing with the installation positions for windows on the top and on the lateral side, as well as the film injector subassembly and the base plate, which is fixed to the setup via clamping plates at the bottom. The channel housing is made of aluminium alloy; the base plate is made of copper. Before starting a test, its temperature can be adjusted via dedicated heater pads which are glued to the base plate.

The lateral windows can be installed at dedicated ports which are distributed equidistant along the channel axis. The vertical position of the windows allows a flush alignment of the window with the bottom of the channel in order to properly resolve the cooling film height with the optical diagnostics. The location of the top window takes into account that due to the limitation of the test time and the time it takes for the Laser-induced Fluorescence (LIF) temperature images to be taken, the optical temperature measurement cannot be performed along the entire channel length during one test run. Moreover, the LIF measurement is of interest only in the region where the film is heated from injection temperature to saturation temperature.
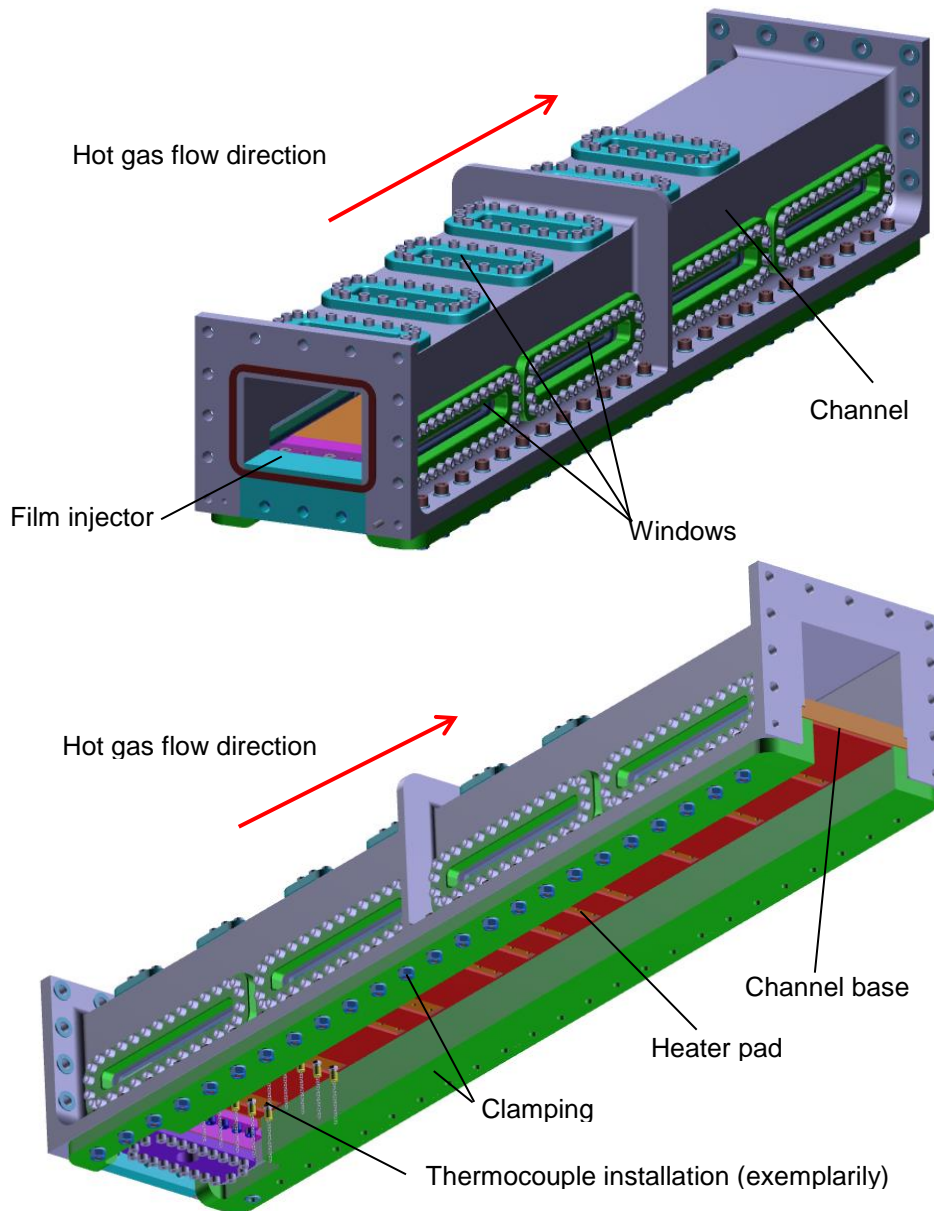
Figure 4: Test section

The injector is fixed to the channel from the bottom. The cover of the injector, which forms the annular passage through which the coolant is injected into the measurement section, is fixed to the body by screws from below.

First CFD simulations have shown that the design of the coolant manifold and the routing of the coolant inside the injector provide a homogeneous distribution of the film to the injector orifices. Subsequently, various CFD simulations were run by ArianeGroup and Numeca to address the following issues:

- Effect of the detailed design of the coolant manifold upper volume on the homogeneity of the injected film
- Effect of injection geometry - discrete bores vs. continuous slot on film quality
- Effect of size of rearward facing step above injector on flow topology of film
- Effect of ramp angle downstream of film injector on film homogeneity and entrainment

For the design of the coolant manifold, the result of the simulations suggested modifying the geometry of the injector manifold to avoid secondary flows or regions of stationary vortex structures or regions of stagnation. The design limits also as far as possible the heat transfer from the hot gas flowing over the injector plate to the coolant fluid inside the manifold. Stainless steel was selected as material for this part to limit its thermal conductivity. The use of ceramic material to further reduce the heat input was discarded due to its limited machinability, its thermal expansion coefficient (which would not match to the rest of the setup), its availability and procurement lead time.

Figure 5 illustrates the investigations on the effect of the orifice geometry on the transient evolution of the film quality performed by Numeca. Whereas a configuration with discrete injection bores (as shown in the left image in Figure 5) would be more representative of the later application in a liquid rocket engine, where the liquid cooling jets potentially would impact under an oblique angle onto the combustion chamber wall, a continuous slot (like the one shown in the right image of Figure 5) results in a more homogeneous and well-controlled injection profile. This is better suited for fundamental code validation purposes focussing on the heat and momentum exchange further downstream. Consequently, it was decided to proceed with a configuration using a continuous slot.

Figure 6 illustrates simulations performed by ArianeGroup on the effect of the thickness of the injector cover on the interaction of the hot gas flow and the liquid film downstream of the injector. The thickness of the injector cover defines the height of the rearward facing step at the injector, which induces a vortex structure impinging on the liquid film. From a numerical point of view, an infinitesimal thin step would be desirable. In real applications in liquid rocket engines, the flow structure is far more complex with the film being injected through discrete bores and very large recirculation zones of combustion gases close to the injector face plate. In the experiment the film cover was designed as thin as seems reasonable from an engineering point of view, given the fact that the top cover shall be machined at limited cost and shall provide sufficient mechanical strength against thermal dilatation.

The design of the coolant manifold aims at minimising the heat input to the coolant fluid through the thin-edged cover plate to avoid local boiling of the ethanol due to the heat impact from the cover plate. As the film injector's cover is planned to be installed flush with the bottom floor of the experiment, its overall height directly influences the angle of the ramp, across which the film is injected to the film cooled wall. As with the injector cover, an infinitesimal height would be desirable. The slot height and the thickness of the lip chosen for the final configuration result in a ramp angle of just below 1.5°.

Table 2 lists the geometry parameters of the film injection slot.
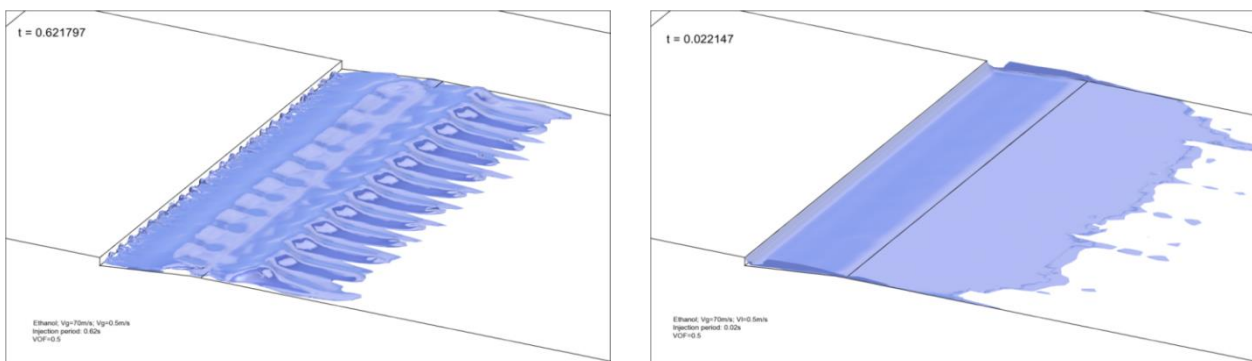

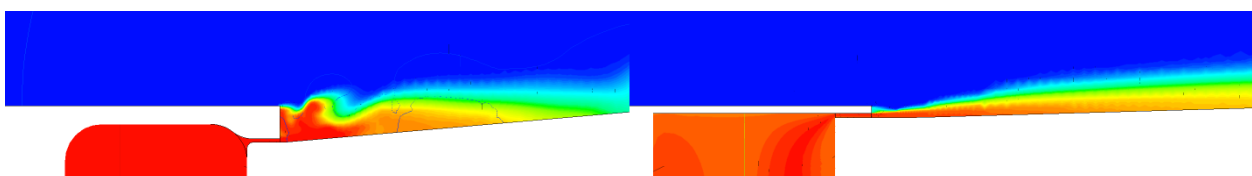Figure 5:   Flow simulation by Numeca: 23 discrete bores vs. continuous slot

Figure 6:   ArianeGroup assessment of effect of thickness of rearward facing step

Table 2: Film injector parameters

Parameter	Symbol	Value
Slot height	h	0.25 mm
Lip thickness / cover thickness	t	0.40 mm
Slot width	w	100 mm
Ramp angle	α	1.5°

The channel base plate to which the film is injected is designed as an uncooled copper plate. It is set to a pre-defined bulk temperature before the start of the experiment in order to make use of the thermal inertia of the massive copper plate and heat up the floor plate prior to the test. The required range of temperature is limited by the saturation temperature of the coolant fluid. In all test cases, the difference between the hot gas temperature and the film temperature will be significantly higher than the temperature difference between the film and the wall, so that the potential heat flux from the channel wall to the film is subordinate to the heat input form the hot gas.

The use of electrically heated pads which are glued to the lower surface of the copper plate can provide the required structure temperature in approximately 15 minutes. The heating power required is in the range of 0.7 kW to 2 kW. Before and during the test, the structure temperature was monitored with numerous type K thermocouples, which are installed in the bottom floor. The sheathed thermocouples feature an isolated measurement tip to avoid electric interference with the metallic test setup. They are installed in bores which end at a distance of 1 mm from the hot gas wall. The location and the spacing of the thermocouple bores are illustrated in Figure 7
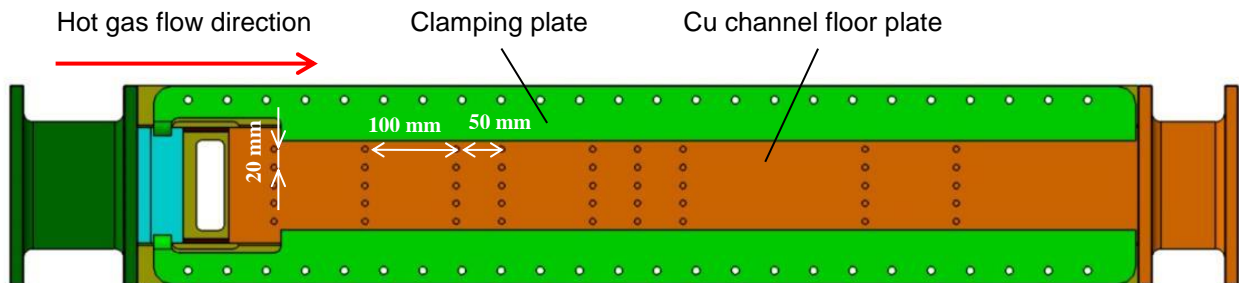

Figure 7:   Channel floor plate with bores for thermocouples (film injector not shown)

2.2   Optical Diagnostics

To increase the quality of the already existing data base on liquid film cooling, the experiments used non-intrusive measurement techniques, which have been developed by VKI and DLR to fit to the experiment's requirements. VKI used a Laser-Induced-Fluorescence (LIF) setup to measure the bulk temperature of the liquid film downstream of the injection slot. DLR applied the so-called Background-Oriented Schlieren (BOS) technology to measure the film thickness independently of the LIF setup.

LIF is a non-intrusive measurement technique, which is based on creation of an unstable energy state of a fluorophore dissolved in a flow, excited by a certain energy wavelength. A detailed description of the LIF technology can be found in [25]. In this setup, the LIF-technology was applied in the so-called 2-Colours-2-Dyes configuration (2C2D), in which two different dyes were used and excited at the same wavelength. This allows eliminating the effects of potential variations of dye concentration due to the evaporation of the liquid film. Another challenge for the LIF temperature measurement was the thin thickness of the film, which was expected to measure around 0.2 mm. To cope with this challenge, extensive calibration tests were performed before the setup was used at the M11.1 test facility. These calibration tests also addressed the long-duration stability of the dyes and the effect of evaporation on the recorded emission spectra.

For this application, a laser beam expanded till a cross section of 20 mm of diameter and directed with an inclination of about 15° illuminated the liquid film, creating an ellipse of light on the liquid interface. The laser used was a Nd:Yag pulsed laser at 30 mJ and repetition rate of 15 Hz of the Litron brand. The collection device was an Ocean Optics spectrometer HR2000 provided with a fibre optic with aperture diameter of 600 µm. The fibre optic on the side of the liquid film was equipped by a spherical lens of 25 mm diameter, focal length of 20 mm and Numerical Aperture of 0.60. The system composed by the fibre optic head and the spherical lens looked from above the liquid film interface with an inclination of about 15°.

The LIF optical test bench designed to operate at the M11.1test facility is shown in Figure 8. Figure 9 illustrates the excitation laser path and the fluorescent emission cone collected by the Top probe. In Figure 10, a picture of the LIF optical test bench mounted in the M11.1facility is presented, where the position of the calibration cell is visible. Indeed, the optical arrangement was such that in order to perform the daily verification of the calibration of the solution, the prism could be turned by 180° and realigned on the calibration cell.
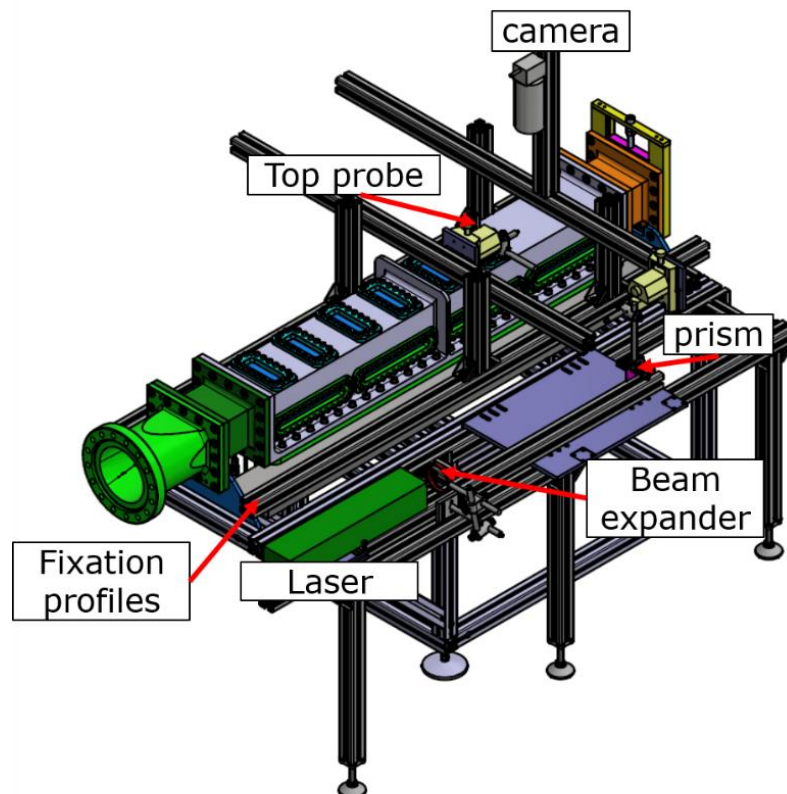

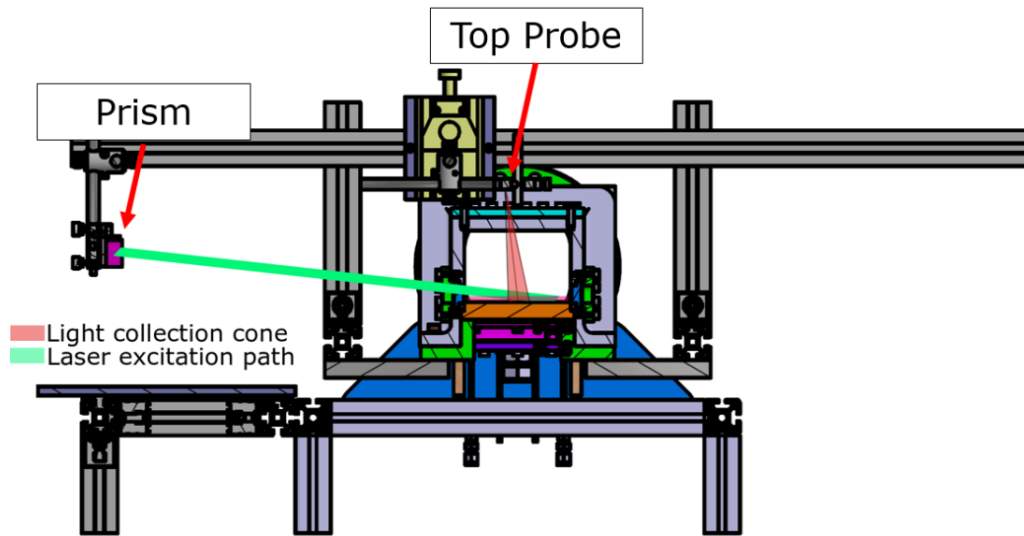Figure 8:   LIF setup configuration

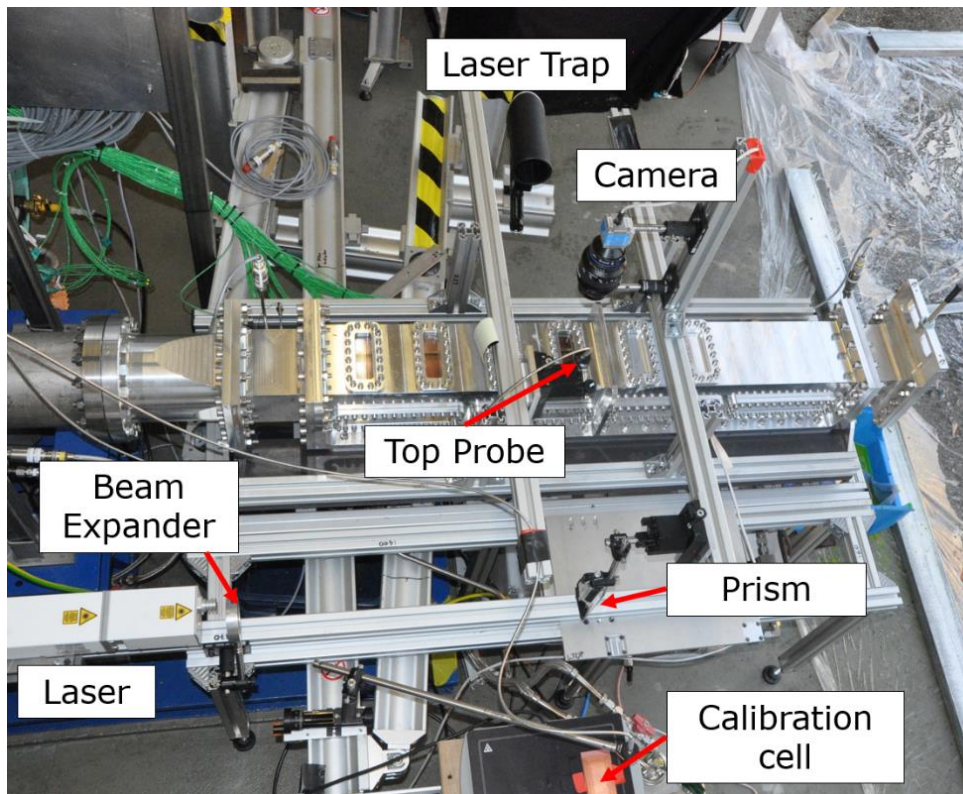Figure 9:   Test setup installed at M11.1test facility

Figure 10:   Test setup installed at M11.1test facility

To provide an additional non-intrusive and independent measurement on the film thickness, DLR installed an optical setup which applied the so-called "Background-Oriented Schlieren" technology. The Background Oriented Schlieren technique also known as 'synthetic Schlieren' ([26] and [27]) is a relatively new flow visualization technique. It has only become available during the last two decades through advances in computational image processing. Like the conventional Schlieren technique it is based on the deflection of light rays by gradients in the refractive index of the medium. However, in contrast to conventional Schlieren techniques the BOS technique has the advantage of a very simple setup and the fact that the field of view is not limited by the size of the optics. The basic principle of a BOS setup can be seen in Figure 11.
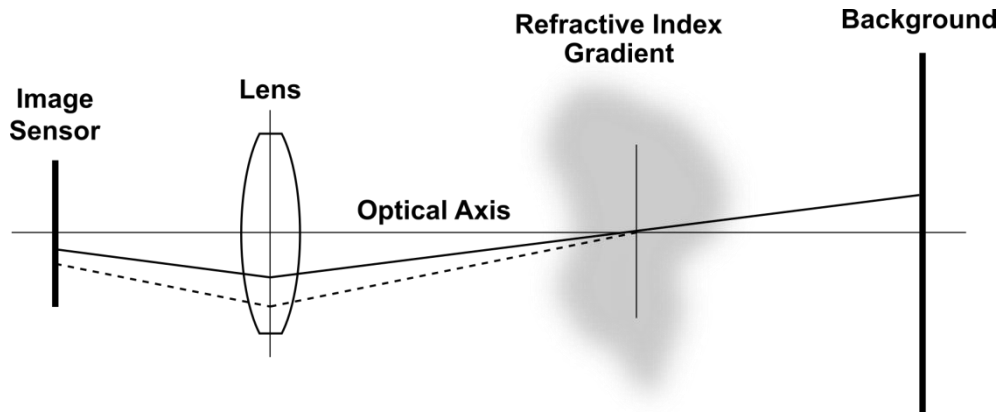
Figure 11:   Background Oriented Schlieren (BOS) Setup Scheme

A special background with a high spatial frequency pattern is recorded by a camera. This background can be e.g. a printed pattern or a laser speckle background. Due to refractive index gradients which are induced by the flow, light rays are deflected by a small angle. This causes a displacement of pixel in the recorded image compared to a reference image without flow. These displacements can then be computed by different image processing algorithms to ultimately create an image of the flow field. DLR Lampoldshausen uses the in-house developed and Matlab-based software BOSVIS, (see Fig. 16) which applies the optical flow algorithm by Horn and Schunck [28] to calculate the flow field. Unlike cross-correlation algorithms, the original resolution of the images is preserved when using optical flow algorithms (see [29]). Furthermore, computational very efficient implementations of this algorithm are already available for Matlab (see [30]). In order to further improve the results of the Horn-Schunck algorithm, additional post processing features have been implemented in the BOSVIS software.
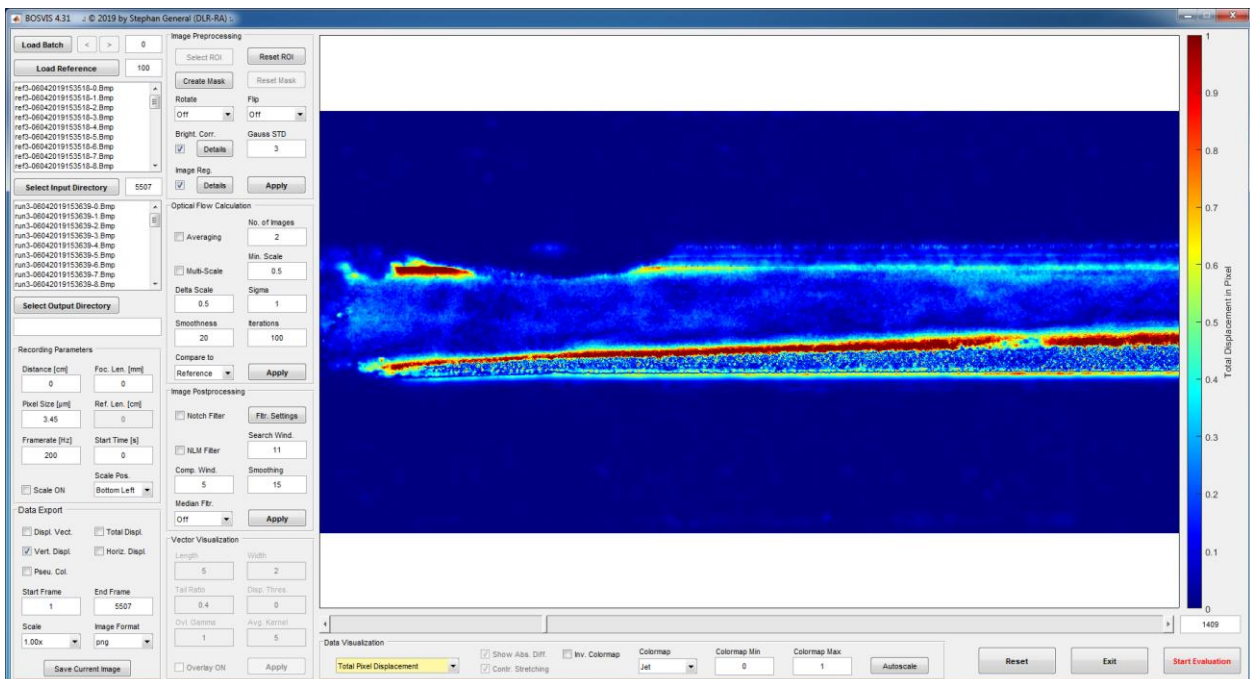

Figure 12:   Screenshot of current BOSVIS software

In order to determine the film thickness preliminary experiments using a Background Oriented Schlieren setup were performed. The BOS test setup consists of an actively cooled array of 30 Cree® XP-E2-Q4 green high power LEDs featuring a total electrical power of more than 100 W, which illuminate a backlit Plexiglas plate with a 1200 dpi high-resolution speckle background. The imaging is done by an industrial CCD camera (FLIR® Blackfly® S BFS-U3-51S5M-C, 200 fps), equipped with a C-mount lens (Fujinon® HF50HA-1B, 1:2,3/50 mm). The LEDs emit green light, since the selected camera is most sensitive in the green spectrum of light. This high performance BOS system has been developed out of a BOS legacy on supersonic flows and Scramjet research at M11.1 (see [28]).

3   Experimental Results

3.1   Operating Conditions

The test campaign was performed between January and June 2019. A first series of tests was performed without film injection to characterise the hot gas system only. These tests provided information on the general behaviour of the setup, the transient characteristics of the test section and the reproducibility of the hot gas conditions.

Subsequently, the tests with different film coolant mass flow rates were performed. Altogether, more than 100 load points were performed, covering various different operating conditions in mass flow rates, pressure and gas temperature. The range of parameters investigated is given in Table 3. The blowing ratio given in the diagram has been calculated as ratio of the momentum flux of the cooling film and of the hot gas:

$$M = \frac{\rho_L \cdot v_L}{\rho_G \cdot v_G}$$

Table 3: Range of experimental parameters

Parameter	Symbol	Values
Hot gas temperature	T_{HG}	500 K; 600 K
Hot gas mass flow rate	$\dot{m}_{HG}$	0.63 kg/s; 1.35 kg/s
Hot gas static pressure	p_{HG}	1 bar; 2 bar
Film mass flow rate	$\dot{m}_{film}$	5 g/s; 10 g/s, 20 g/s; 30 g/s; 40 g/s 60 g/s
Blowing ratio	M	1.5 - 50

Figure 13 shows the operating conditions as a diagram in which the hot gas temperature T_{HG} has been plotted vs. the blowing ratio M.
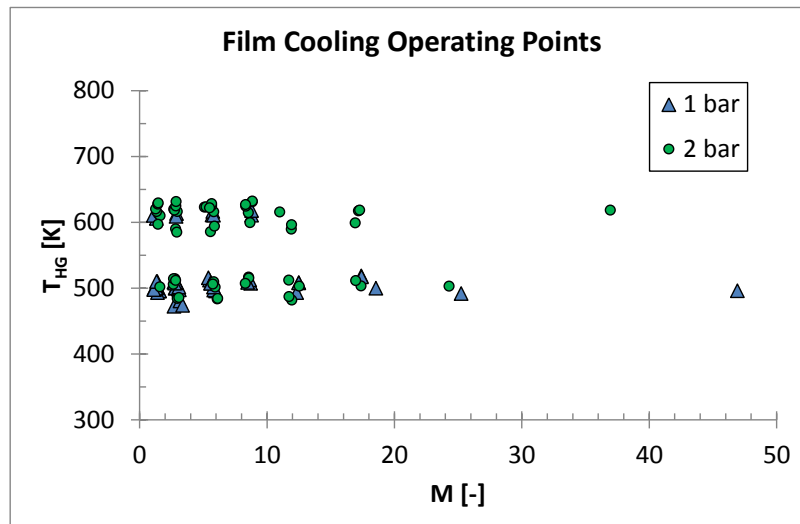

Figure 13:   Film Cooling Operating Conditions: Blowing ratio M vs. pressure and gas temperature

3.2   Wall Temperature Measurements

First results from the thermocouple wall temperature measurements are shown in Figure 14 and Figure 15. The data shown in the diagrams have been recorded in a test with a hot gas mass flow rate of 1.35 kg/s at a temperature of 600 K and a pressure of 2 bar. A film mass flow rate of 10 g/s was injected at ambient temperature. The coolant temperature is measured during the test in the injector manifold and is shown with a black line. A red line shows the

hot gas pressure and indicates a run time of 20 seconds. The measured wall temperatures are given with various colours.

During the test sequence, the cooling film is injected 5 seconds before the hot gas valve is opened in order to properly establish a liquid film before this interacts with the hot gas flow. This results in a noticeable drop of approximately 2 - 3 K in the wall temperature at H_0-5 seconds in all axial positions. Due to heat transfer effects in the film injector manifold, the coolant temperature stabilizes approximately at H_0+3 seconds.
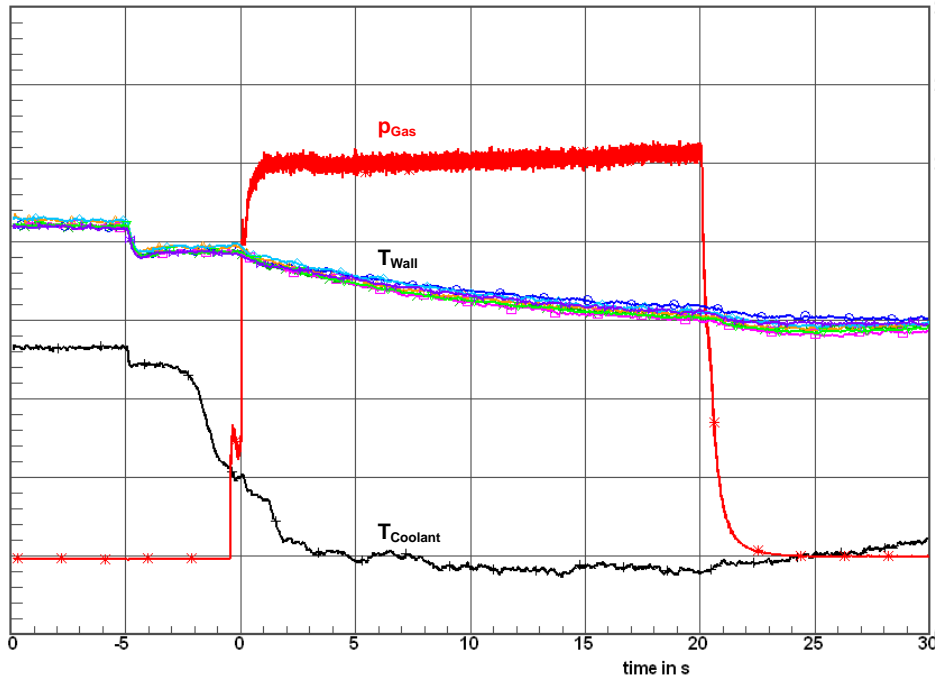

Figure 14: Wall temperature measurements: lateral distribution 50 mm downstream of injector
(Film mass flow rate 10 g/s, gas mass flow rate 1.35 kg/s, gas temperature 600 K)
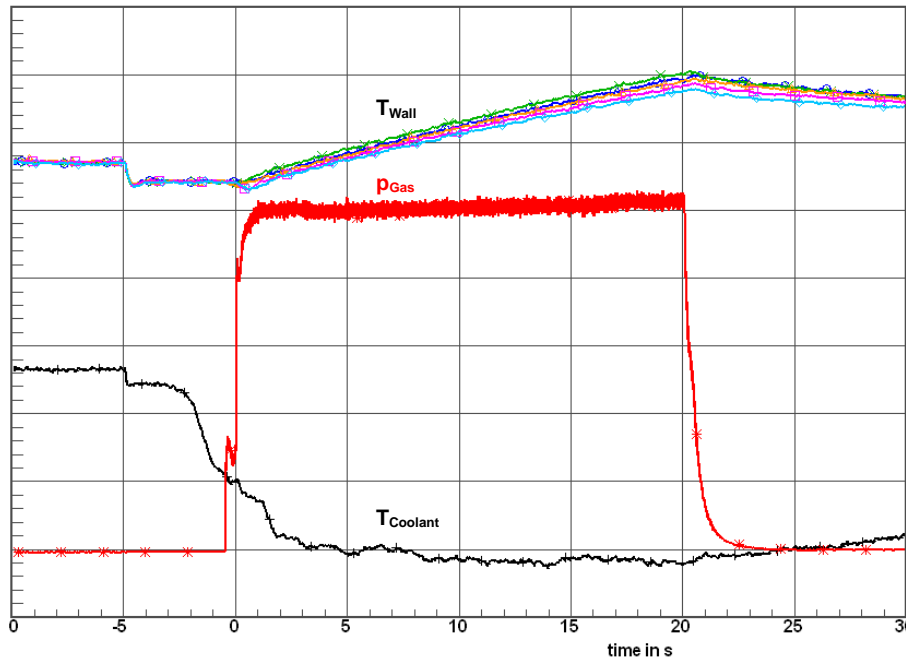

Figure 15: Wall temperature measurements: lateral distribution 500 mm downstream of injector
(Film mass flow rate 10 g/s, gas mass flow rate 1.35 kg/s, gas temperature 600 K)

13

Comparing the wall temperature signals recorded at the two axial positions (50 mm downstream of the injector in Figure 14 and 500 mm downstream of the injector in Figure 15, respectively) show that the wall temperature measurements give a very homogeneous result in span-wise direction with a scatter of less than 2 K at test start. Note that during this test, the initial wall temperature of the bottom wall was not exactly uniform at the beginning of the test due to the heat input from a preceding test run. From the injector to the last measurement position, an increase in the wall temperature of about 15 K was recorded before the start of the test.

Figure 14 shows that at a position 5 mm downstream of the film injector the wall is continuously cooled down by the film injection, approaching a steady-state plateau at H_0+20 seconds, when the test is stopped. In contrast, the wall temperature at a position 500 mm downstream of the injector increases continuously throughout the test (see Figure 15).

Figure 16 illustrates the evolution of the wall temperature along the central axis of the setup. The axial temperature profile of the wall, which is present at the start of the experiment, can clearly be seen before H_0. The decreasing efficiency of the cooling film is illustrated by the different slopes of the temporal evolution of the wall temperature at different axial positions. At the end of the test, the axial temperature gradient only slowly levels out.
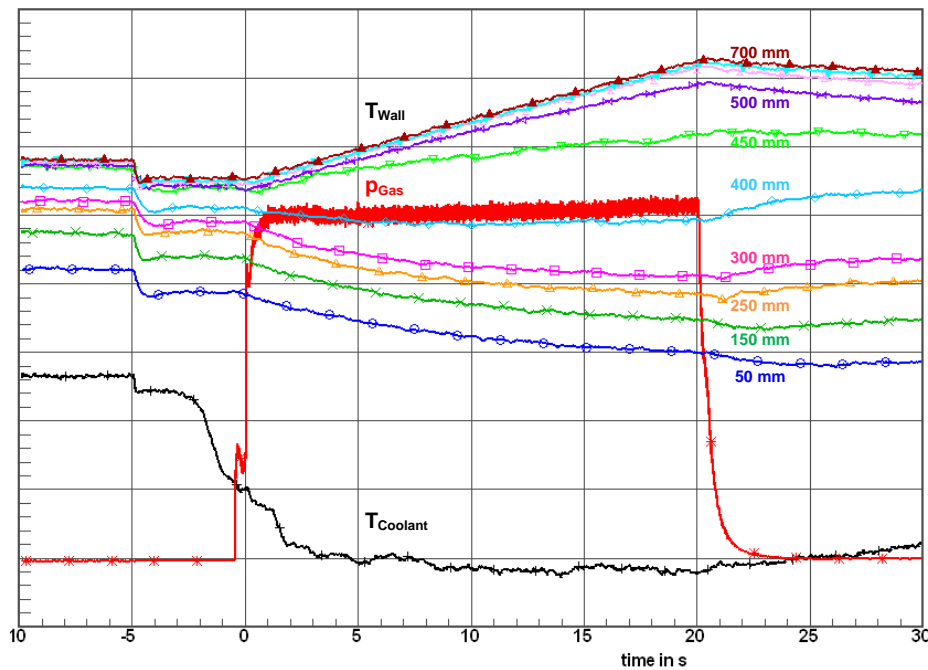

Figure 16:   Wall temperature measurements: axial evolution along centreline from 50 mm to 700 mm downstream of injector (Film mass flow rate 10 g/s, gas mass flow rate 1.35 kg/s, gas temperature 600 K)

3.3   Optical Diagnostics - Film Temperature

First results from LIF technique are presented in Figure 17. The data shown correspond to a position of about 118 mm downstream to the injector and they have been recorded with a hot gas mass flow rate of 1.35 kg/s at a temperature of 600 K and a pressure of 2 bar. Only the data coloured in red were recorded at a testing pressure of 1 bar. The liquid flow rate varies between 5 and 30 g/s. In the plot, markers represent LIF data while continuous lines represent the thermocouple values at a position 150 mm downstream to the injector at the axial position. Additional measurements have been performed at a position 378 mm downstream to the injector with the same test conditions (see Figure 18). For this position, no LIF data were available at a film flow rate of 5 g/s due to an irregular presence of dry-spots, probably located upstream. The available data at 10, 20 and 30 g/s suggest that the liquid temperature is not affected by the film mass flow rate.
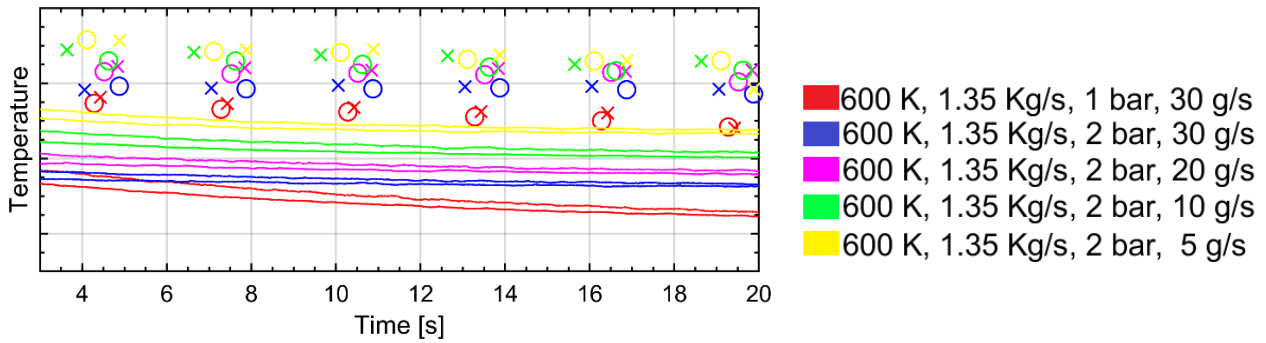
Figure 17: LIF temperature measurements at 118 mm downstream to the injector and corresponding wall temperature measurements at the axis, 150 mm downstream to the injector.
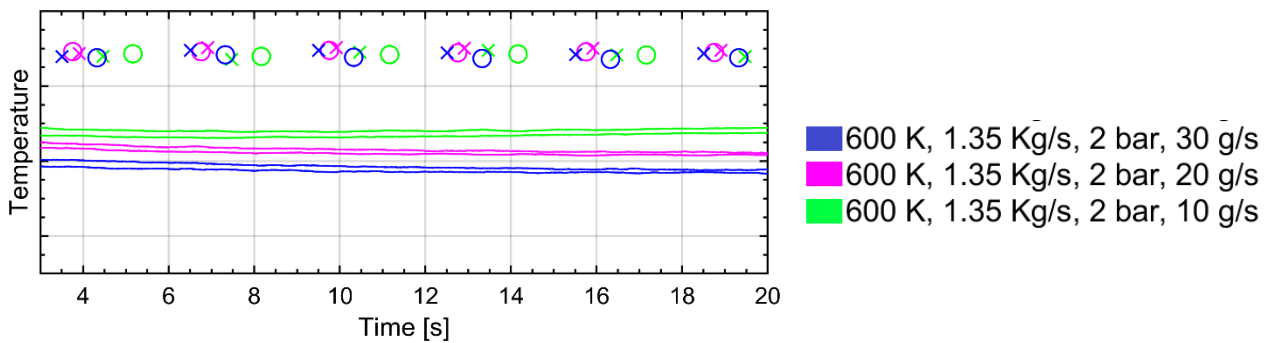

Figure 18: LIF temperature measurements at 378 mm downstream to the injector and corresponding wall temperature measurements at the axis, 400 mm downstream to the injector.

3.4 Optical Diagnostics - Film Thickness

Figures 19 to 21 show preliminary BOS results for a hot run at 600 K stagnation temperature and 2 bar static pressure in the experimental channel as an example. This corresponds to a hot gas mass flow rate of 1.35 kg/s. Ethanol coolant was injected at a rate of 20 g/s into the main flow. The interrogation area shown covers the whole first lateral window with a length of 200 mm and a height of 20 mm. In all images the ramp can be identified on the left hand side with a length of about 20 mm. Furthermore, dark areas appear at the upper left and on both corners of the window. Those areas are cracks in the window caused by thermal stresses on the experimental channel and the resulting thermal expansion. They appear as dark areas, since they obscure the speckle background and therefore get subtracted by the BOSVIS algorithm. Figure 19 shows a sharp border between the coolant boundary layer and the hot gas main flow, which corresponds to the other results gained so far by BOS. They indicate that this method is well applicable for determining the film thickness. Figures 20 and 21 show that the main displacement takes place in the vertical direction, whereas only small displacements are found in the horizontal direction.

Further BOS results indicate an inhomogeneous coolant boundary layer with surface waves and evaporation, which is currently under investigation but might have an effect on the LIF measurements that needs to be compensated.
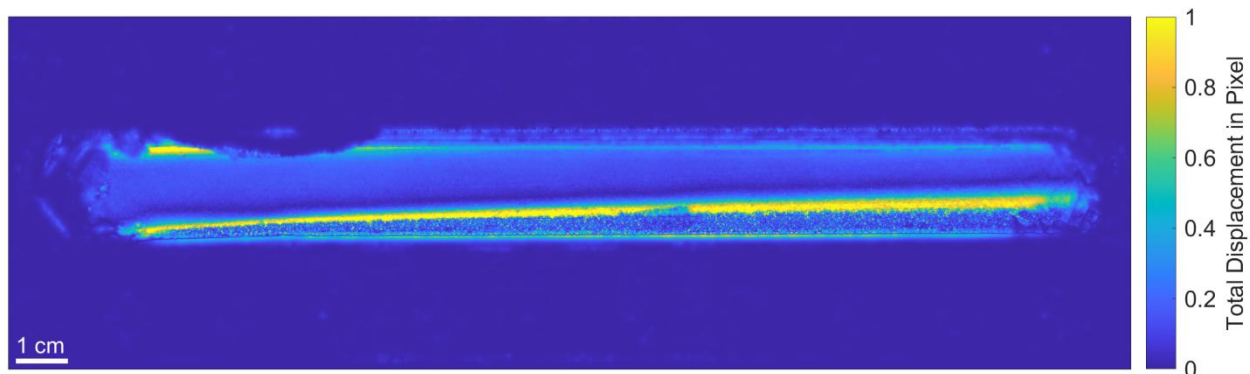

Figure 19: BOS total displacement image of ethanol coolant film at
600 K, 2 bar, 1.35 kg/s and 20 g/s coolant mass flow rate, 1st lateral window
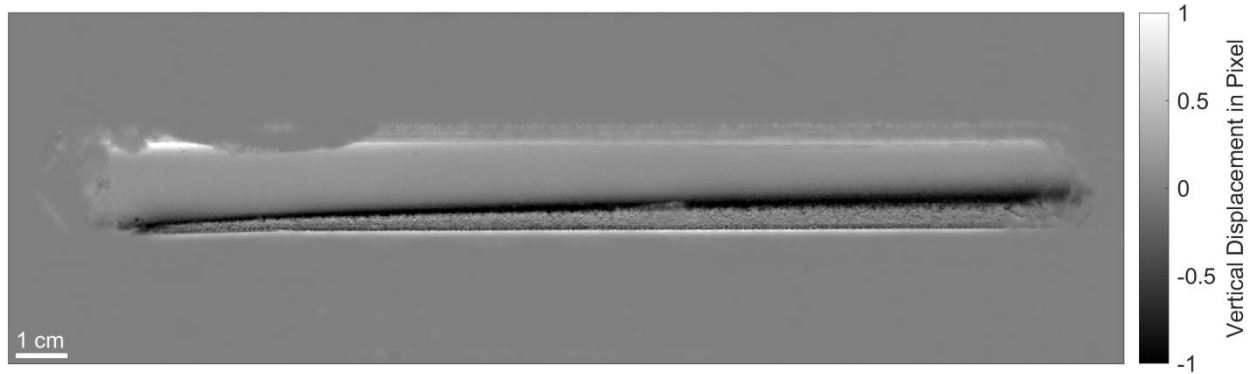
15

Figure 20: BOS vertical displacement image of ethanol coolant film at
600 K, 2 bar, 1.35 kg/s and 20 g/s coolant mass flow rate, 1st lateral window
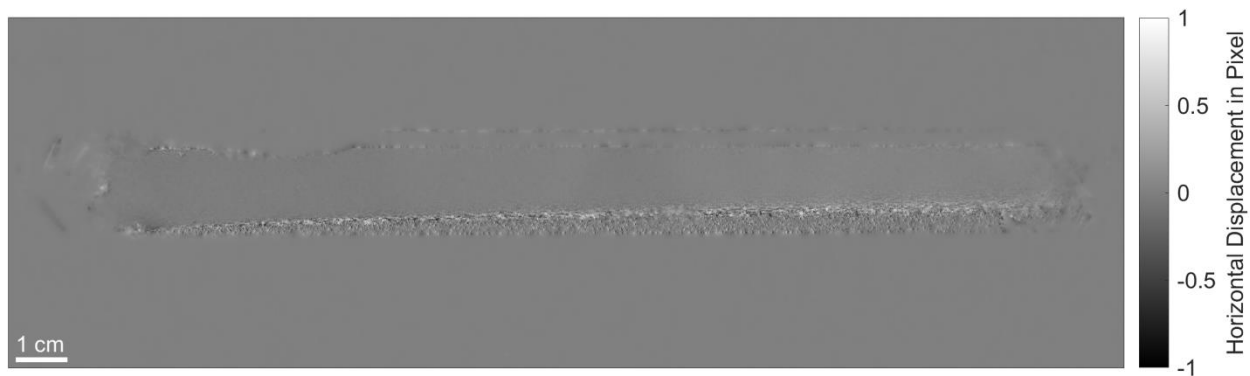

Figure 21: BOS horizontal displacement image of ethanol coolant film at
600 K, 2 bar, 1.35 kg/s and 20 g/s coolant mass flow rate, 1st lateral window

4   Discussion of Results

More than 100 individual load points have been recorded, providing a sound data base for the validation of engineering and high-fidelity simulation models. A detailed analysis of all the test data is currently in progress. In parallel, simulations at ArianeGroup and Numeca are being performed to validate the individual CFD codes against dedicated test cases, which have been derived from the experimental data base. As soon as these simulations are finished, a comparison of the simulation and the experimental results will be published.

An experimental data base for liquid ethanol cooling films has been established. The test data recorded at different operating conditions allow for assessing the effect not only of mass flow rate and temperature of the hot gas and the film coolant, but also of the pressure and of the wall temperature of the wall under the cooling film. Wall temperature measurement was successfully performed at various axial and lateral positions in the cooled wall. Non-intrusive LIF-based temperature measurements of the liquid cooling film have been performed successfully.

A first qualitative analysis of the test data showed that the data base allows for quantifying the effect of operating parameters like the gas mass flow rate, temperature and pressure on the film behaviour. The measured wall temperatures indicate an effect of the film mass flow rate of the axial temperature gradient. A quantitative assessment of the data has not been performed yet. As expected, the LIF temperature measured at the first axial position shows an effect of the cooling efficiency and hence on the difference between wall temperature and film temperature. For a more detailed analysis, the offset of the initial wall temperature values in the different tests needs to be taken into account. The same applies for the effect of the operating pressure, which can be assessed in Figure 17 when comparing the blue and the red symbols. Data seem to indicate that in the case with the lower pressure the heat input into the film and the wall is lower, resulting in a better cooling performance of the film. Again, a more detailed analysis of the data is required before definite conclusions can be drawn.

At a position of 378 mm downstream of the film injection, the comparison of LIF-based film temperature measurement and wall temperature values measured with the thermocouples shows a clear effect of the film mass flow rate on the cooling efficiency of the film: With increasing film mass flow rate, the difference between wall temperature and film temperature increases. Again, the effect of initially different wall temperature levels needs to be taken into account for a more detailed quantitative analysis. The fact that the liquid film temperature does not vary in this position for the different film mass flow rates indicates that the ethanol has reached its saturation temperature in this position. Here, a detailed comparison of the measured temperature with the theoretical saturation temperature at the static pressure in the experiment needs to be performed; the latter increases from 351 K to 370 K with an increase in pressure from 1 bar to 2 bar.

The experiments showed that achieving steady state wall temperature conditions was not quite straightforward during the tests. The heating pads could be used to deliberately modify the wall temperature at the start of the experiment. However, the comparatively high mass of the floor plate provided significant thermal inertia, which was visible as axial temperature gradient at test start in some of the experiments. For the validation of simulation models, the axial wall temperature profile needs to be taken into account.

For high film mass flow rates, the interaction of the cooling film with the hot gas resulted in a noticeable reduction of the hot gas bulk temperature, which was measured before the exit of the test section. Whether this is attributed to evaporation effects only or additional effects of entrainment of film fluid in the hot gas core flow is currently being investigated. Such effects have been detected by BOS; but since the data is still undergoing post-processing the results of this analysis will be included in future publications

5   Summary

Within a test series at the M11.1 air vitiator test facility of DLR Lampoldshausen, liquid film cooling tests have been performed using liquid ethanol as film fluid. The film fluid, as well as, the operating conditions were selected to be representative of operating conditions in a small rocket combustion chamber. The tests deliberately aimed at avoiding a chemical interaction of the hot gas and the cooling film; instead the design of the experiment focusses on the interaction of a shear-driven liquid film subjected to heat transfer.

The tests used thermocouples to monitor the film cooled wall temperature during the test. Additionally, the von-Karman-Institute performed in-situ temperature measurement of the film using a specially calibrated LIF setup. DLR developed a setup to perform a Background-Oriented Schlieren measurement of the film thickness along the channel floor.

The test data can be used to assess the film efficiency along the channel wall for various operating conditions and serves as a data base for the validation of numerical models which are currently being developed at Numeca.

6   Outlook

Dedicated load points will be selected as reference test cases for the validation of numerical models of Numeca and ArianeGroup. Whilst ArianeGroup focuses on the anchoring and improvement of its 3D-Navier-Stokes solver Rocflam3, Numeca is currently updating the multiphase flow simulation capabilities of its Fine[TM]/Open with OpenLabs[TM] integrated environment to take into account effects of heat transfer and evaporation.

7   Acknowledgements

8   References

[1]   G. R. Kinney and J. L. Abramson,, "Internal-liquid-film-cooling Experiments with Air Stream Temperatures to 2000°F in 2- and 4-inch-diameter Horizontal Tubes," 1952.

[2]   A. E. Abramson, "Investigation of Internal Film Cooling of Exhaust Nozzle of a 1000-pound-thrust Liquid-ammonia Liquid-oxygen Rocket," 1952.

[3]   G. Morrell, "Investigation of Internal Film Cooling of 1000-pound-thrust Liquid-ammonia-liquid-oxygen Rocket-engine Combustion Chamber," 1951.

[4]   Y. C. Yu, R. Z. Schuff and W. E. Anderson, "Liquid Film Cooling Using Swirl in Rocket Combustors," 2004.

[5]   G. R. Kinney, J. L. Abramson and J. L. Sloop, "Internal-liquid-film-cooling Experiments with Air Stream Temperatures to 2000°F in 2- and 4-inch-diameter Horizontal Tubes," 1952.

[6]   C. Höglauer, "{Filmkühlungsmodellierung in Raketenschubkammern}," 2015.

[7]   R. Arnold, "Experimentelle Untersuchungen zur Filmkühlung in Raketenbrennkammern," 2008.

[8]   D. M. Kercher, "A Film Cooling CFD Bibliography," *International Journal of Rotating Machinery,* vol. 4, pp. 61-72, 1998.

[9]   H. A. Zuniga, V. Krishnan and J. S. Kapat, "Effect of Non-Symmetrical Lateral Diffusion on Film Cooling Effectiveness from a Row of Shaped Holes," 2008.

[10] K. H. Dellimore, C. Cruz, A. W. Marshall and C. P. Cadou, "A Jet Model for Slot Film Cooling with Effect of Variation in the Mainstream Pressure," 2007.

[11] K. M. Kirk and H. Merte, "A Mixed Natural/Forced Convection Nucleate Boiling Heat Transfer Criteria," 1994.

[12] K. M. Kirk, H. Merte and H. Keller, "Low-velocity Subcooled Nucleate Flow Boiling at Various Orientations," *J. Heat Transfer,* vol. 117, pp. 380-386, 1995.

[13] W. E. Welsh, "Review of Results of an Early Rocket Engine Film-Cooling Investigation at the Jet Propulsion Laboratory," 1961.

[14] R. C. Stechman, J. Oberstone and J. C. Howell, "Design Criteria for Film Cooling for Small Liquid-Propellant Rocket Engines," Journal of Spacecraft and Rockets, vol. 6, pp. 97-102, 1969.

[15] J. E. Hatch and S. R. Papell, "Use of a Theoretical Flow Model to Correlate Data for Film Cooling or Heating an Adiabatic Wall by Tangential Injection of Gases of Different Fluid Properties," 1959.

[16] G. Schlieben, C. Kirchberger, H.-P. Kau, C. Höglauer and O. Knab, "Film Cooling Investigations within a GOX/Kerosene Combustion Chamber," 2011.

[17] Welsh, "Review of Results of an Early Rocket Engine Film-Cooling Investigation at the Jet Propulsion Laboratory", 1962

[18] Nahstoll, "Untersuchungen von Flüssigkeits-Filmströmungen bei hohen Verdampfungsraten im Hinblick auf Filmkühlung", 1988

[19] Haberlen, P. A.; Greisen, D. A.; Anderson, W. E., A Film Cooling Model for a RP-1/GOX Staged Combustion Liquid Rocket Engine, 2007

[20] C. F. Warner and D. L. Emmons, "Effects of Selected Gas Stream Parameters and Coolant Properties on Liquid Film Cooling," Journal of Heat Transfer, vol. 86, pp. 271-278, 1964.

[21] M. R. Gater and M. R. L'Ecuyer, "A Fundamental Investigation of The Phenomena That Characterize Liquid Film Cooling," 1969.

[22] J.-G. Kim, K.-J. Lee, S. Seo, Y.-M. Han, H.-J. Kim and H.-S. Choi, "Film Cooling Effects on Wall Heat Flux of a Liquid Propellant Combustion Chamber," 2006.

[23] F. Strauss, C. Manfletti, D. Freudenmann, J. Witte, and S. Schlechtriem, "Preliminary Experiments on Transpiration Cooling in Ramjets and Scramjets," AIAA 2016-4968, American Institute of Aeronautics and Astronautics, 2016

[24] F. Strauss, M. Woessner, M. Weisswange, C. Manfletti, and S. Schlechtriem, "Experiments on Flow Interaction in a Transpiration Cooled Model Scramjet," 7th European Conference of Aeronautics and Space Sciences (EUCASS), July 3rd–6th, 2017, Milan, Italy. EUCASS 2017-235, 2017. doi: 10.13009/EUCASS2017-235

[25] A. Simonini, D. Fiorini, L. Peveroni, J-B. Gouriet, S. Soller, J. Steelant, 2C2D-LIF temperature measurements in a micrometric evaporating film," 14th International Conference on "Two-Phase Systems

for Space and Ground Applications", Granada (Spain), September 24-27, 2019

[26] Dalziel S., Hughes G. and Sutherland B., (2000) Whole-Field Density Measurements by 'Synthetic Schlieren' Exp Fluids, 28(4), pp. 322–335

[27] Settles, G. S., and Hargather, M., "A Review of Recent Developments in Schlieren and Shadowgraph Techniques," Measurement Science and Technology, Vol. 28, 042001, 2017. doi:10.1088/1361-6501/aa5748

[28] Horn, B. K. P. and Schunck, B. G., (1981) Determining Optical Flow, Artificial Intelligence, 17(1-3), pp. 185-203. DOI: 10.1016/0004-3702(81)90024-2

[29] Hayasaka, K., Tagawa, Y., Liu, T. and Kameda, M., (2016) Optical-Flow-Based Background-Oriented Schlieren Technique for Measuring a Laser-Induced Underwater Shock Wave, Experiments in Fluids, 57(179). DOI: 10.1007/s00348-016-2271-0

[30] Kharbat, M., Horn-Schunck Optical Flow Method, v 1.1.0.0, (2009), accessed August 17th, 2018 from https://de.mathworks.com/matlabcentral/fileexchange/22756-horn-schunck-optical-flow-method